ACS APPLIED ENGINEERING MATERIALS

pubs.acs.org/acsaenm Article

Selenorhodamine-Sensitized $CuAlO_2$ Photocathodes That Reduce Protons to Hydrogen under Visible Illumination

Michael D. Clark, Zachery A. Schmidt, Gregory J. Lapp, Hannah R. Dierolf, Kacie Liwosz,* and David F. Watson*

Cite This: *ACS Appl. Eng. Mater.* 2024, 2, 2190−2200 Read Online

ACCESS | Metrics & More | Article Recommendations | Supporting Information

ABSTRACT: We prepared dye-sensitized photocathodes (DSPs) by attaching a phosphonic acid-functionalized selenorhodamine dye (3-SeP) to delafossite $CuAlO_2$ thin films. The dye 3-SeP adsorbed to $CuAlO_2$ as a mixture of monomeric and H-aggregated dyes, broadening the dye's absorption profile and enhancing the absorption of visible light. Upon exposure to solvent, 3-SeP persisted on $CuAlO_2$ to a much greater extent than analogous selenorhodamines either bearing a terminal carboxylic acid group or lacking a surface-anchoring group. Transient photovoltage measurements revealed a long-lived positive shift of the Fermi level of 3-SeP/$CuAlO_2$-on-FTO electrodes, consistent with a mechanism in which holes are transferred from photoexcited 3-SeP to $CuAlO_2$. In linear sweep voltammetry measurements under chopped white-light illumination, 3-SeP/$CuAlO_2$-on-FTO electrodes exhibited 7- to-8-fold greater reductive photocurrents than unfunctionalized $CuAlO_2$-on-FTO electrodes, revealing that excited-state hole transfer and the resulting separation of photogenerated holes from electrons could be exploited to promote reduction and oxidation half reactions. In prolonged-illumination chronocoulometry experiments, 3-SeP/$CuAlO_2$-on-FTO electrodes, in conjunction with a Co(III) reduction cocatalyst and triethanolamine as a sacrificial electron donor, reduced H^+ to H_2 with Faradaic efficiency of 43 ± 27%. Our results highlight the potential of selenorhodamine-sensitized Cu(I) delafossites as DSPs for redox photocatalysis and the production of solar fuels.

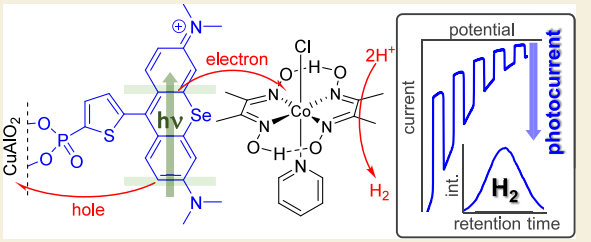

KEYWORDS: *dye-sensitized photocathodes, Cu(I) delafossites, hydrogen evolution reaction, solar photocatalysis, rhodamines*

INTRODUCTION

Dye-sensitized photocathodes (DSPs) are intriguing constructs for solar energy conversion, via the photocatalytic production of fuels or as photocathodes of tandem and *p*-type dye-sensitized solar cells (DSSCs).[1−4] The operating mechanism of DSPs[1−3,5] involves the absorption of light by a sensitizer followed by the transfer of a hole to a *p*-type semiconductor substrate and the transfer of an electron to a reduction cocatalyst or solvated acceptor. The photogenerated hole diffuses to the back contact of the DSP and ultimately oxidizes an electron donor, either at a dark anode, in *p*-type DSSCs or dye-sensitized photoelectrochemical cells (DSPECs), or at a photoanode in tandem DSSCs. Nickel(II) oxide (NiO) is the most extensively reported *p*-type semiconductor for DSPs;[1,4−8] however, several factors have limited the efficiencies of DSSCs and DSPECs with NiO-sensitized photocathodes. Nanostructured NiO films exhibit low hole-diffusion coefficients and poor hole mobility, as well as a relatively high-energy valence band edge that limits the open-circuit photovoltages of DSSCs and the oxidizing potential for photocatalysis.[1,5,8,9] Additionally, rapid charge recombination across the sensitizer/NiO and NiO/electrolyte interfaces can limit the charge-collection efficiencies of DSSCs and the quantum yields of photocatalysis.[5−7]

Wide-bandgap Cu(I) delafossite compounds, with chemical formula $CuMO_2$ where M is metal cation with oxidation state of +3 (e.g., Al, Ga, Sc, Cr, or Co), have emerged as promising alternative *p*-type semiconductors for DSPs.[1,3,7,9,10] Relative to NiO, $CuMO_2$ compounds exhibit lower-energy valence band edges and improved hole mobilities due to the delocalization of valence-band states across oxygen and copper.[1,9,10] Several groups have recently reported on redox photocatalysis mediated by $CuMO_2$-derived DSPs within a DSPEC configuration. Kumagai et al. adsorbed a supramolecular Ru(II)−Re(I) photocatalyst to high-surface-area $CuGaO_2$ films to yield DSPs that photocatalytically reduced CO_2 to CO.[11] Windle et al. coimmobilized a push−pull organic dye and a cobaloxime reduction catalyst on $CuGaO_2$ films, and the resulting DSPs reduced protons to hydrogen with Faradaic efficiency of 74%.[12] Similarly, Reisner and co-workers coimmobilized phosphonic acid-functionalized organic dyes

Received: June 3, 2024
Revised: July 12, 2024
Accepted: July 15, 2024
Published: July 23, 2024

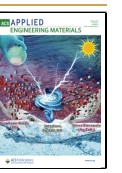

https://doi.org/10.1021/acsaenm.4c00368
ACS Appl. Eng. Mater. 2024, 2, 2190−2200

and a Ni(II) cocatalyst onto $CuCrO_2$ electrodes to yield DSPs that reduced protons to hydrogen with Faradaic efficiencies of 25−45%.[13,14] These reports highlight the potential of $CuMO_2$-derived DSPs in redox photocatalysis.

Our research groups have contributed to a collaborative effort to develop chalcogenorhodamine dyes as sensitizers in *n*-type DSSCs and for homogeneous and heterogeneous redox photocatalysis.[15−20] Selenorhodamines are particularly attractive as sensitizers because they exhibit red-shifted absorption bands relative to analogous oxygen-containing rhodamines, which enhances the absorption of visible light, and because they undergo efficient intersystem crossing to yield long-lived triplet excited states.[15,20−22] Under appropriate conditions, carboxylated and phosphonated selenorhodamine dyes adsorb to surfaces as mixtures of monomers and H-aggregates, which broadens absorption spectra and enhances light-harvesting efficiency.[17,20] Remarkably, in *n*-type sensitization schemes, H-aggregation of selenorhodamines also enhances electron-injection yields, probably due to the enforced coplanarity of the xanthylium core and the aryl group of dyes within aggregates.[15,16,18,19] McCormick et al. reported that a selenorhodamine sensitizer, together with a solvated cobaloxime cocatalyst (Co-cat, Chart 1) and triethanolamine (TEOA)

Chart 1. Structures of (a) Selenorhodamine Dyes TMR-Se, 1-SeC, and 3-SeP, Which Consist of a Common Selenoxanthylium Core (*xan*, Bottom) Functionalized at the 9 Position with Variable Aryl Groups (*Ar*, Top), and (b) the Cobaloxime Co-catalyst (Co-cat)

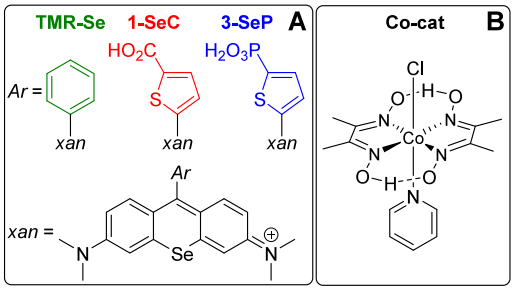

as sacrificial reductant, photocatalytically evolved hydrogen from aqueous solutions with remarkably high turnover number (9000) and quantum yield (32.8%).[21] Photophysical measurements supported a mechanism in which TEOA reduced the photoexcited selenorhodamine dye, which then reduced the Co(III) catalyst to initiate the hydrogen-evolution reaction (HER). The selenorhodamine dye outperformed analogous sulfur- and oxygen-containing dyes in photocatalytic HER. McCormick et al. attributed this result to the selenorhodamine dye's high quantum yield of intersystem crossing, which populated a triplet excited state that was sufficiently long-lived for reductive quenching by TEOA to outcompete radiative and nonradiative relaxation of the dye.[21]

Inspired by the promise of selenorhodamine sensitizers in photocatalytic hydrogen evolution, and of Cu(I) delafossites as hole-accepting substrates in DSPs, we endeavored to sensitize $CuMO_2$ thin films with selenorhodamine dyes to yield DSPs for photocatalytic hydrogen evolution. Notably, DSPs can be coupled with a range of oxidation half-reactions that occur at a dark anode, potentially eliminating the need to consume sacrificial electron donors. We focused initially on $CuAlO_2$ because its bandgap and band-edge potentials are optimal,[1,7,9,23−26] syntheses of $CuAlO_2$ films have been reported,[26−29] and $CuAlO_2$ has been used as a hole-accepting semiconductor in DSPs for *p*-type and tandem DSSCs.[28,30,31]

In this article, we report on the preparation of selenorhodamine-functionalized $CuAlO_2$ thin films and the exploration, using photoelectrochemical methods, of their excited-state charge-transfer reactivity and performance as DSPs, via a *p*-type sensitization mechanism, in reductive photocatalysis. We discovered that a phosphonic acid-bearing selenorhodamine dye, 3-SeP (Chart 1),[17,20] is particularly inert on $CuAlO_2$, and that photoexcited 3-SeP transfers holes to $CuAlO_2$ and can reduce a cobaloxime catalyst to initiate the reduction of protons to hydrogen. This line of research represents an initial example of dye-sensitized $CuAlO_2$ DSPs. Our results thus highlight the potential of DSPs derived from selenorhodamines, with relatively low-energy absorption bands and long-lived triplet excited states that facilitate excited-state charge transfer, and Cu(I) delafossites in redox photocatalysis and fuel-forming photochemistry.

EXPERIMENTAL SECTION

Materials

Reagents were obtained from the following commercial sources: (1) Acros Organics [4-*N*,*N*-dimethylbenzoic acid (98%), triethylamine (99%), ethylene glycol (99%)]; (2) Alfa Aesar [phosphorus(V) oxychloride (99%), *N*,*N*,*N*′*N*′-tetramethylethylenediamine (98%), hexafluorophosphoric acid (aqueous solution, 60% by weight), diisopropylamine (99%), thiophene-2-carboxylic acid (99%), potassium nitrate (KNO_3) (99%)]; (3) Sigma-Aldrich [thionyl chloride (99%), diethylamine (99%), 3-bromo-*N*,*N*-dimethylaniline (97%), iodine (99.8%), selenium powder (99.5%), *sec*-butyllithium (cyclohexane solution, 1.4 M), bromobenzene (99%), *n*-butyllithium (hexanes solution, 2.5 M), chlorotrimethylsilane (99%), sodium iodide (99.5%), aluminum nitrate nonahydrate ($Al(NO_3)_3{\cdot}9H_2O$) (98%), copper(II) nitrate ($Cu(NO_3)_2{\cdot}2.5H_2O$) (98%), citric acid (99%), polyethylene glycol (PEG), lactic acid (LA) (85%), triethanolamine (TEOA) (98%), chloro(pyridine)bis(dimethylglyoximato)cobalt(III) (Co-cat), potassium chloride (KCl) (99%)]; (4) Fisher [magnesium turnings (99%)]; (5) TCI [tetrabutylammonium hexafluorophosphate ($TBAPF_6$) (98%)]. Dichloromethane, tetrahydrofuran, ethanol, and acetonitrile (CH_3CN) were obtained from various commercial sources. All reagents and solvents were used as received.

Syntheses of Chalcogenorhodamine Dyes

Three dyes were synthesized as described previously: TMR-Se,[32] 1-SeC,[33] and 3-SeP[17] (Chart 1).

Synthesis of $CuAlO_2$ Thin Films

$CuAlO_2$ films were synthesized by adaptation of the procedure reported by Jarman et al.[27] Separate 1.00 M aqueous solutions of Al^{3+} and Cu^{2+} were prepared by dissolving $Al(NO_3)_3{\cdot}9H_2O$ (15.0 g, 40.0 mmol) and $Cu(NO_3)_2{\cdot}2.5H_2O$ (9.30 g, 40.0 mmol) in deionized H_2O (diH_2O) (40.0 mL). These solutions of Al^{3+} and Cu^{2+} were combined, and then citric acid (76.8 g, 0.400 mol) was added to yield a solution with 1:1:10 molar ratio of Al^{3+} to Cu^{2+} to citric acid. Ethylene glycol (4.46 mL, 80.0 mmol) was dissolved into this solution, and the resulting reaction mixture was heated at 200 °C until liquids evaporated, which yielded a brown solid. The solid was ground with a mortar and pestle and then heated in a muffle furnace at 500 °C for 4 h under ambient atmosphere. The resulting black powder was cooled to room temperature and then heated at 1100 °C for 4 h in a tube furnace, under ambient atmosphere, to yield blue-gray $CuAlO_2$ powder. To prepare thin films, $CuAlO_2$ powder (0.50 g), polyethylene glycol (PEG) (0.10 g), ethanol (2.50 mL), and diH_2O (1.25 mL) were combined and stirred until the PEG dissolved. The resulting mixture was spray-coated, using a Master Airbrush (Model

https://doi.org/10.1021/acsaenm.4c00368
ACS Appl. Eng. Mater. 2024, 2, 2190−2200

679) at a pressure of 60 lb in^{-2}, onto either glass microscope slides (for dye-adsorption experiments) or FTO-coated glass slides (for photoelectrochemical experiments), which were placed on a metal block surface on top of a hot plate held at 220 °C.

Adsorption of Dyes to $CuAlO_2$ Thin Films

$CuAlO_2$ films on glass or FTO-coated glass slides were functionalized with TMR-Se, 1-SeC, or 3-SeP (Chart 1) by immersion in CH_3CN solutions of the dye (0.1−3.5 mM) for 16−24 h. Slides were removed, rinsed twice by immersion in neat CH_3CN, allowed to dry, and then characterized by diffuse reflectance UV/vis absorption spectroscopy. The net contributions of the dyes to diffuse reflectance spectra were calculated by subtracting the spectrum of the bare $CuAlO_2$ film, acquired before immersion of the film into the dye solution, from the spectrum of the dye-functionalized $CuAlO_2$ film.

Materials Characterization Methods

Scanning electron microscopy (SEM) images were acquired with a Hitachi SU70 field emission instrument with an Oxford Inca SDD energy dispersive spectroscopy (EDS) detector. X-ray powder diffraction (XRD) data for $CuAlO_2$ powders were acquired with a Rigaku Ultima IV X-ray diffractometer operating with Cu Kα radiation (λ = 0.154 nm) and scanning from 20° to 80°. UV/vis absorption spectra of solvated dyes were acquired with an Agilent 8453 spectrometer. Diffuse reflectance UV/vis spectra of $CuAlO_2$ and dye-functionalized $CuAlO_2$ thin films were acquired using the same spectrophotometer with a Labsphere RSA-HP-53 reflectance accessory.

Transient Photovoltage Experiments

Two-electrode cells, with a 3-SeP-functionalized $CuAlO_2$-on-FTO working electrode (WE) and a Pt mesh counter electrode (CE), were assembled in a custom single-compartment 500 μL Teflon cell, which was filled with neat CH_3CN that had been purged with Ar for approximately 10 min. A 0.478 cm^2 region of the WE was exposed to CH_3CN. Under open-circuit conditions, the 3-SeP/$CuAlO_2$ electrode was illuminated concurrently with (a) CW white light (190 mW cm^{-2}), from a 100 W Xe lamp (Oriel Photomax) output through a filter that transmitted 420−700 nm light, and (b) pulsed 532 nm light ((1.2 ± 0.2) mJ cm^{-2}, 6−8 ns pulse width, 1 Hz repetition rate, ∼ 1 cm^2 diameter) from the frequency-doubled output of a Continuum Powerlite Precision II Nd:YAG laser. The voltage difference between the WE and CE was measured by a LeCroy Waverunner 6050 oscilloscope, and net transient photovoltages were calculated as the difference between the laser pulse-induced voltage and the baseline voltage under CW illumination.

Cyclic Voltammetry (CV), Linear Sweep Voltammetry (LSV), and Chronocoulometry

The electrochemical responses of $CuAlO_2$ and 3-SeP-functionalized $CuAlO_2$ thin films, in the dark and under white-light illumination, were measured using CV, LSV, and chronocoulometry. Data were acquired with a Princeton Applied Research (PAR) VersaSTAT 3 potentiostat. The WE was an FTO electrode coated with $CuAlO_2$ or dye-functionalized $CuAlO_2$, the CE was Pt mesh, and the reference electrode (RE) was a saturated calomel electrode (SCE). Electrodes were housed in either a sealed 100 mL 3-neck round-bottomed flask (single-compartment cell) or a sealed custom H-cell (3-compartment cell). Several different supporting electrolytes were used, as described in the Results and Discussion section. Unless otherwise noted, for both cell configurations, the electrolyte and headspace were deaerated prior to the acquisition of data by purging with Ar for 1 h. In CV measurements, the scan rate was 100 mV s^{-1}, whereas in LSV measurements, the scan rate was 10 mV s^{-1}. In LSV measurements involving chopped illumination, the WE was illuminated with a white LED (20 mW cm^{-2}) for 5 s and then kept in the dark for 5 s, and this cycle was repeated throughout the measurement. In prolonged-illumination chronocoulometry experiments involving chopped illumination, unless otherwise noted the WE was illuminated with white light for 10 min and then held in the dark for 5 min, and this cycle was repeated throughout the measurement. The light source was a 100 W Xe arc lamp (Oriel Photomax) output through a filter that transmitted 400−720 nm light (400 mW cm^{-2}). After prolonged illumination, the headspace above the electrolyte in the WE compartment was analyzed for the possible formation of H_2 using a PerkinElmer Clarus 580 gas chromatograph with a thermal conductivity detector and Ar as carrier gas.

RESULTS AND DISCUSSION

Interfacial Energetic Offsets Driving Excited-State Hole Transfer and Photocatalysis

We envisioned a photocatalytic mechanism initiated by the transfer of holes from photoexcited selenorhodamine dyes to $CuAlO_2$. The thermodynamic favorability of this hole-injection process is dictated by the energetic offset between the valence band edge of $CuAlO_2$ and the hole-donor (or electron-acceptor) distribution function of the selenorhodamine, which is centered at $G° + \lambda$, where $G°$ is the free energy corresponding to the ground-state oxidation potential of the dye and λ is the hole-transfer reorganization energy.[34,35] Reported valence band-edge potentials of $CuAlO_2$ range from +0.7 to +0.9 V vs NHE,[7,9,36,37] and the measured ground-state oxidation potential ($E_{1/2}^{2+/+}$) of 1-SeC is +1.35 V vs NHE.[15] (We assume similar $E_{1/2}^{2+/+}$ values for TMR-Se and 3-SeP; reported $E_{1/2}^{2+/+}$ values of chalcogenorhodamines are insensitive to functionalization of the thienyl group with carboxylic or phosphonic acids.[38]) Therefore, assuming a λ value of 0.2−0.6 eV,[39,40] some or all of the hole-donor distribution function of the selenorhodamine dyes should lie lower in energy than the valence band edge of $CuAlO_2$, rendering excited-state hole injection thermodynamically favorable. In contrast, the conduction band-edge potential of $CuAlO_2$ (−2.0 to −2.5 V vs NHE)[9,37] is 1.3 to 1.9 V more negative than the excited-state oxidation potential ($E_{1/2}^{2+/+*}$) of the selenorhodamine dyes (−0.64 V vs SCE for 1-SeC);[15] therefore, electron injection from the photoexcited dyes to the conduction band of $CuAlO_2$ is thermodynamically unfavorable. McCormick et al. reported that photoexcited and/or reduced selenorhodamine dyes can reduce Co-cat, the cobaloxime cocatalyst, which in turn can reduce protons to H_2.[21] This result, together with the interfacial energetic offsets driving hole injection, underpins our targeted mechanism of photocatalytic HER, which is outlined in Scheme 1.

Synthesis and Characterization of $CuAlO_2$ Thin Films

We synthesized $CuAlO_2$ via the Pechini method,[41] wherein metal cations are chelated by citrate and the resulting complexes are then reacted with ethylene glycol to yield, via esterification, a polymeric metal-containing resin that yields the

Scheme 1. Simplified Targeted Photocatalytic Mechanism, in Which the Transfer of Holes from Photoexcited 3-SeP to $CuAlO_2$ Enables the Reduction of Co-cat and Then H^+

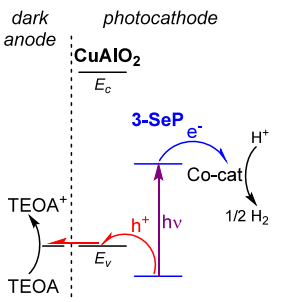

https://doi.org/10.1021/acsaenm.4c00368
ACS Appl. Eng. Mater. 2024, 2, 2190−2200

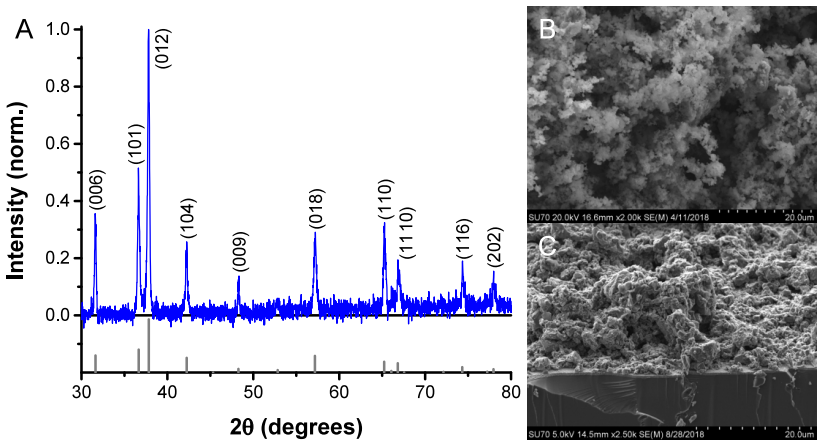

Figure 1. (A) Measured X-ray diffraction (XRD) pattern of $CuAlO_2$ (blue data, top); peaks are indexed to ICDD card #04−007−8058 for delafossite $CuAlO_2$ (gray, bottom); (B) SEM image of $CuAlO_2$ powder; (C) cross-sectional SEM image of spray-deposited $CuAlO_2$ thin film.

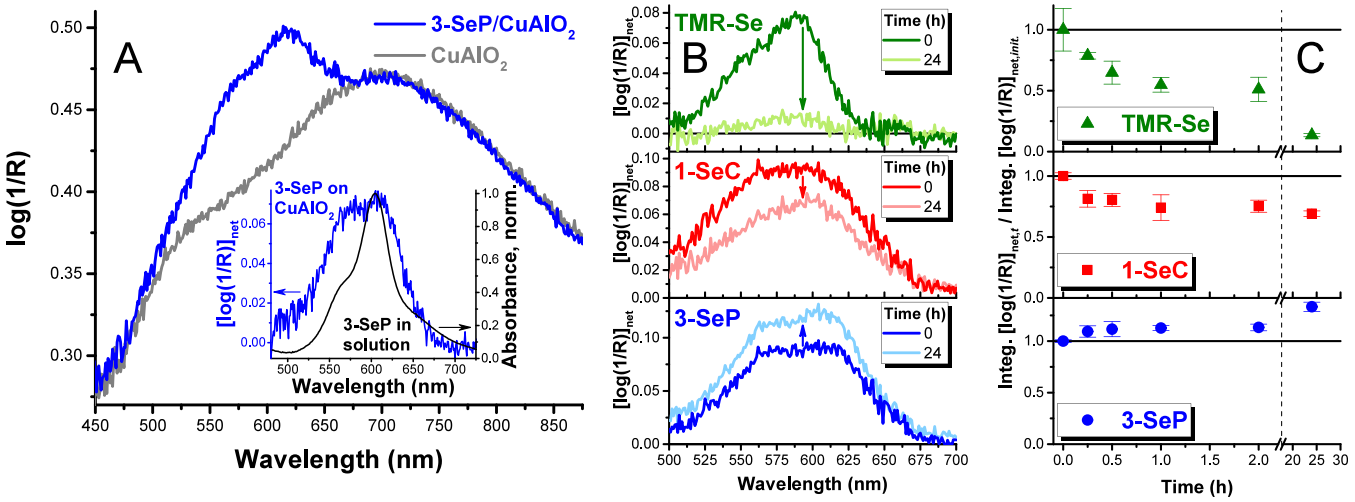

Figure 2. (A) Diffuse reflectance UV/vis spectra of $CuAlO_2$ and 3-SeP-functionalized $CuAlO_2$ thin films (each spectrum is the average from three films); *inset:* net apparent absorbance ($[\log(1/R)]_{net}$) of $CuAlO_2$-adsorbed 3-SeP, calculated by subtracting the spectrum of $CuAlO_2$ from that of 3-SeP-functionalized $CuAlO_2$, overlaid with the absorbance spectrum of a solution of 3-SeP in CH_3CN. (B) Net apparent absorbance spectra of TMR-Se, 1-SeC, and 3-SeP, adsorbed to $CuAlO_2$ films, before and after immersion for 24 h in neat CH_3CN. (C) Estimated fractional surface coverages of TMR-Se, 1-SeC, and 3-SeP on $CuAlO_2$ films, calculated by dividing the net apparent absorbance of the dye by the time-zero value, as a function of immersion time (t) in neat CH_3CN; error bars correspond to plus-or-minus one standard deviation relative to the average of two films per data point.

metal oxide upon heating.[42,43] To synthesize $CuAlO_2$, we reacted nitrate salts of Cu(II) and Al(III) with citric acid and ethylene glycol, by modification of the procedure reported by Jarman et al.[27] The XRD pattern of the resulting powders (Figure 1a) matched reported measured and simulated patterns,[26,44] as well as ICDD (International Centre for Diffraction Data) pattern #04−007−8058, for delafossite $CuAlO_2$. The XRD pattern contained no discernible peaks attributable to CuO (e.g., at 2θ = 35.6° or 38.8°) or $CuAl_2O_4$ (e.g., at 2θ = 45.0° or 59.5°).[27] EDS spectra of $CuAlO_2$ powders (Figure S1 in Supporting Information) revealed a Cu:Al molar ratio of 0.98 ± 0.02. Thus, XRD and EDS data provide evidence for the synthesis of phase-pure delafossite $CuAlO_2$. SEM images of $CuAlO_2$ powder reveal crystallites with dimensions of 0.1−1 μm (Figure 1b and Figure S1). Spray deposition of suspended $CuAlO_2$ powders onto FTO-coated glass yielded high-surface-area gray films with thicknesses on the order of 10^{-6}−10^{-5} m (Figure 1 and Figure S1). Diffuse reflectance UV/vis spectra of $CuAlO_2$ films exhibited a broad absorption throughout the visible and into the near-IR with a maximum at 700 nm and a higher-energy shoulder centered at approximately 534 nm (Figure 2a).

Functionalization of $CuAlO_2$ Films with Selenorhodamine Dyes

$CuAlO_2$-coated glass slides were immersed in acetonitrile solutions of TMR-Se, 1-SeC, and 3-SeP and allowed to equilibrate. After exposure to the dyes, the diffuse reflectance spectra of $CuAlO_2$ thin films exhibited a new absorption band extending from 500 to 700 nm with an absorption maximum at 590−605 nm and a higher-energy shoulder centered at 560−575 nm (Figure 2a,b). For each dye, the new absorption band overlapped with the visible absorption profile of the solvated dye, but with enhanced absorption within the higher-energy shoulder (Figure 2a, inset). Blue-shifted absorption is a hallmark of H-aggregation of dyes.[45,46] Thus, the presence of these broadened, blue-shifted absorption bands of the dyes in the spectra of dye-exposed $CuAlO_2$ films reveals (a) that TMR-Se, 1-SeC, and 3-SeP adsorbed to $CuAlO_2$ and (b) that the

https://doi.org/10.1021/acsaenm.4c00368
ACS Appl. Eng. Mater. 2024, 2, 2190−2200

dyes were present on the surface as mixtures of monomeric and H-aggregated dyes, as we have reported previously for chalcogenorhodamine dyes on nanocrystalline TiO_2 and ZrO_2 films.[16,17,20]

DSPs require inert, persistent dye−semiconductor linkages. To evaluate the persistence of the dyes on $CuAlO_2$, we immersed dye-functionalized $CuAlO_2$ films in neat acetonitrile and periodically acquired diffuse reflectance spectra of the films (Figure 2b,c). Fractional surface coverages of dyes on $CuAlO_2$ were estimated by dividing the integrated net apparent absorbance at a given immersion time ($[\log(1/R)]_{net,t}$) by the initial integrated net apparent absorbance ($[\log(1/R)]_{net,init.}$) measured at the outset of desorption experiments.

TMR-Se desorbed essentially completely from $CuAlO_2$ after being immersed in acetonitrile for 1 day. The lability of TMR-Se is unsurprising given the dye's lack of an anchoring group for covalent or coordinate covalent bonding to $CuAlO_2$. In contrast, approximately 70% of 1-SeC, which presumably adsorbed to $CuAlO_2$ as the deprotonated dye via the carboxylate group, was retained on $CuAlO_2$ after being immersed in acetonitrile for 1 day. The absorbance in the high-energy shoulder (585−615 nm) of 1-SeC decreased relative to the absorbance in the lower-energy (565−585 nm) band, revealing a decrease in the amount of H-aggregated dyes relative to monomeric dyes.

Dye 3-SeP, which presumably adsorbed to $CuAlO_2$ as the deprotonated dye through the phosphonate group, did not desorb upon prolonged exposure to acetonitrile. Interestingly, the estimated fractional surface coverage of 3-SeP actually increased by 33% after 24 h of immersion in acetonitrile. We tentatively attribute the measured increase of net apparent absorbance ($[\log(1/R)]_{net}$) of $CuAlO_2$-adsorbed 3-SeP to an increase of the integrated molar absorption coefficient of the dye arising from a change of local environment (liquid CH_3CN vs air) and/or an evolution of the average orientation or aggregation state of the dye on the $CuAlO_2$ surface. The ratio of the absorbances at the maxima of the low-energy (595−615 nm) and high-energy (570−590 nm) bands of 3-SeP increased by approximately 10%, consistent with a slight decrease in the extent of H-aggregation of 3-SeP on $CuAlO_2$ during the immersion in acetonitrile. We have previously reported subtle changes in the extent of aggregation of chalcogenorhodamine dyes on metal oxides during prolonged exposure to solvents.[20]

The most significant result from these desorption experiments, with respect to selecting a system for photochemical studies, is that 3-SeP persisted on the surface of $CuAlO_2$ during prolonged immersion in acetonitrile. This result is consistent with recent computational studies by Fatihi et al.,[47] who reported that calculated adsorption energies for methylphosphonic acid were 18-to-33% greater than for benzoic acid, on both the pristine (012) surface of $CuAlO_2$ and a (012) surface with Cu(I) vacancies. The greater adsorption energy of the phosphonic acid, relative to the carboxylic acid, would give rise to an increased activation energy for desorption, which is consistent with our experimental data revealing that 3-SeP is more inert than 1-Se-1 on $CuAlO_2$. We and others have reported on the persistence of phosphonic acid-functionalized dyes and ligands on various binary metal oxide surfaces;[17,20,48,49] however, we are unaware of systematic experimental studies of the relative inertness or lability of carboxylic acid- vs phosphonic acid-functionalized adsorbates on $CuMO_2$ surfaces. Our data reveal that phosphonic acid-functionalized dyes are significantly more inert than corresponding carboxylic acid-functionalized dyes on $CuAlO_2$ and, more generally, that phosphonic acids are optimal surface-anchoring groups for $CuMO_2$-derived DSPs. Given the inertness of the 3-SeP/$CuAlO_2$ interface, we used 3-SeP-functionalized $CuAlO_2$ electrodes for photoelectrochemical experiments to evaluate excited-state charge transfer and redox photocatalysis.

Finally, in order to estimate the amount of adsorbed 3-SeP per projected surface area of $CuAlO_2$, hereafter referred to as the "surface coverage" of the dye, we immersed 3-SeP-functionalized $CuAlO_2$ films in acidified (pH 3) water/acetonitrile (90/10 v:v) solutions. Under sufficiently acidic conditions, 3-SeP desorbed from $CuAlO_2$. We could thus quantify the amount of solvated dye from transmission-mode UV/vis absorbance measurements and the reported molar absorptivity of 3-SeP (Figure S2 in Supporting Information).[17] On the basis of these measurements, the estimated surface coverage of 3-SeP on $CuAlO_2$ thin films was 3.5×10^{-7} mol cm^{-2}.

Transient Photovoltage (TPV) Experiments

We used TPV measurements[50−53] to characterize light-initiated processes at 3-SeP/$CuAlO_2$-on-FTO electrodes, with the goal of elucidating the mechanism(s) of any active excited-state charge-transfer processes. In our TPV experiments, a two-electrode photoelectrochemical cell, with a 3-SeP/$CuAlO_2$-on-FTO WE and a platinum CE, was initially held at open circuit under continuous wave (CW) white-light illumination. The cell was then perturbed by illuminating the 3-SeP/$CuAlO_2$-on-FTO WE with a short (6−8 ns) pulse of 532 nm light, within the visible absorption band of the dye (Figure 2), giving rise to a change in the measured open-circuit voltage (V_{oc}). The TPV signal, which we express as ΔV_{oc}, the difference between the time-dependent V_{oc} following pulsed excitation and the steady-state V_{oc} under CW illumination, was then recorded as the cell reestablished equilibrium. The sign of ΔV_{oc} thus reveals whether pulsed excitation of the 3-SeP/$CuAlO_2$ WE resulted in a negative shift ($\Delta V_{oc} < 0$) or positive shift ($\Delta V_{oc} > 0$) of the Fermi level (E_F) of FTO. Decay kinetics of the ΔV_{oc} signal in TPV measurements can depend on CW light intensity (and thus charge-carrier density and the baseline V_{oc}), the population of bulk and surface trap states, capacitive effects, shunt resistance, and finally the rate of charge-carrier recombination across the dye−semiconductor interface.[52,53] Given this complexity, our primary objective in performing TPV experiments was to determine, on the basis of the sign of ΔV_{oc}, whether photoexcited 3-SeP transferred holes to $CuAlO_2$ as envisioned in the targeted photocatalytic mechanism in Scheme 1.

Photovoltage transients for 3-SeP-functionalized $CuAlO_2$ consisted initially of a negative ΔV_{oc} signal, which decayed within 10^{-2} s to a longer-lived positive ΔV_{oc} (Figure 3). Inset A of Figure 3 highlights the decay of the positive signal. The time evolution of the photovoltage transient was well-modeled by a multiexponential kinetic model involving triexponential decay of the initial negative ΔV_{oc} signal, with amplitude-weighted average lifetime of 2.64×10^{-3} s, and mono-exponential decay of the longer-lived positive ΔV_{oc} signal, with lifetime of 1.59 s. The multiexponential kinetic model and fitting parameters are summarized in Appendix S1 in Supporting Information, and a fit is superimposed on the data in Figure 3. The steady-state V_{oc} under CW illumination was 0.095 V; thus, the initial ΔV_{oc} of −0.034 V corresponds to a perturbation of 36% relative to the baseline voltage.

https://doi.org/10.1021/acsaenm.4c00368
ACS Appl. Eng. Mater. 2024, 2, 2190−2200

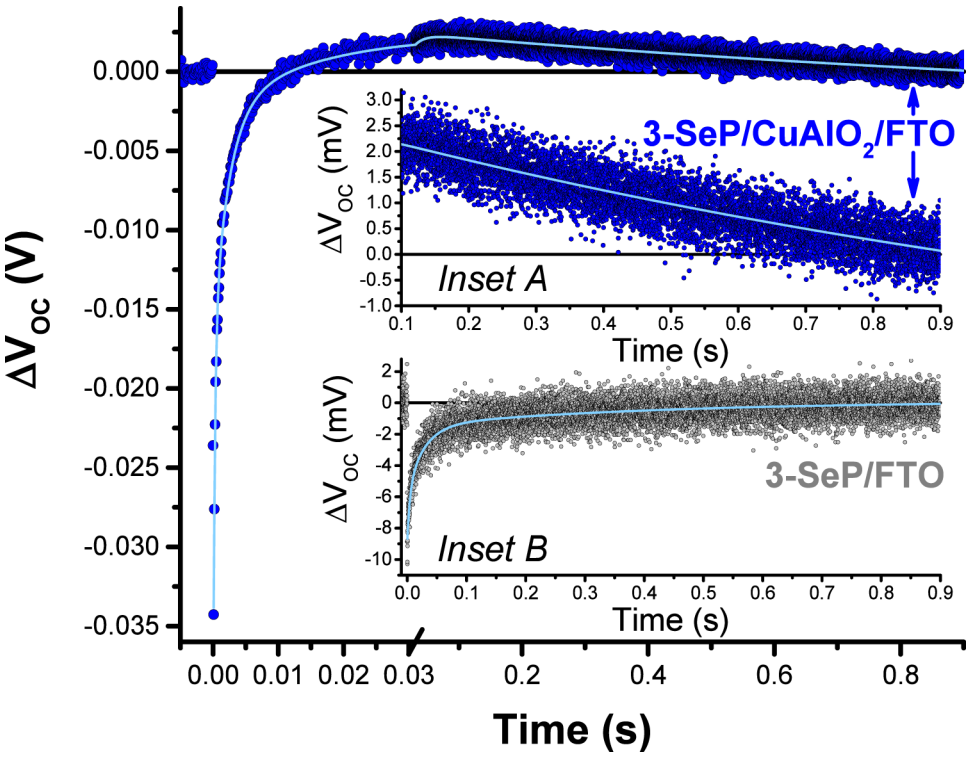

Figure 3. Photovoltage transients for 3-SeP/$CuAlO_2$-on-FTO (main figure and *inset* A) and 3-SeP/FTO (*inset* B) electrodes, where ΔV_{oc} equals the difference between the time-dependent V_{oc} following pulsed 532 nm excitation and the steady-state V_{oc} under CW white-light illumination. Superimposed on the data are fits to multiexponential decay kinetics. The multiexponential kinetic model and fitting parameters are summarized in Appendix S1 in Supporting Information.

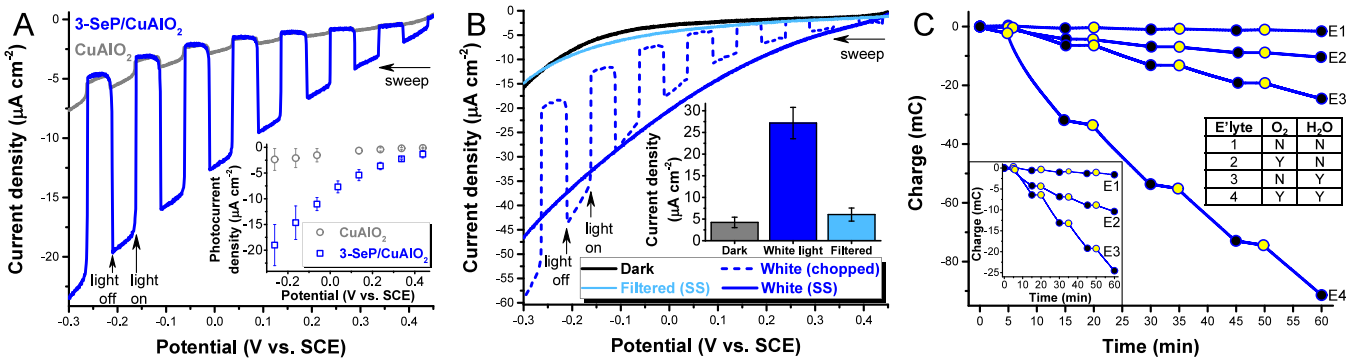

Figure 4. (A) Linear sweep voltammograms of $CuAlO_2$- and 3-SeP/$CuAlO_2$-on-FTO electrodes under chopped white-light (400−720 nm) illumination; *inset:* Average net photocurrent densities as a function of applied potential where error bars correspond to plus-or-minus one standard deviation relative to the average of measurements on 3 different electrodes per sample. (B) Linear sweep voltammograms of 3-SeP/$CuAlO_2$-on-FTO electrodes acquired in the dark, under chopped and steady-state (SS) white light (400−720 nm) illumination, and under illumination through a notch filter that absorbed light from 500 to 700 nm; *inset:* Average current densities in the dark and under steady-state white-light and filtered illumination at an applied potential of −0.10 V vs SCE. (C) Chronocoulometry data for 3-SeP/$CuAlO_2$-on-FTO electrodes under alternating illumination (white light, 400−720 nm) and dark periods, with four different electrolytes (E1-E4) as defined in the text and summarized in the table; black data points represent the start of dark periods, and yellow data points represent the start of illumination periods. *Inset:* zoomed-in graph highlighting chronocoulometry data for electrolytes E1-E3.

Multiexponential voltage-decay kinetics are typical for ΔV_{oc} amplitudes exceeding 5−10% of the steady-state V_{oc}.[51,53] We acquired data with a significant laser-induced perturbation to improve the signal-to-noise ratio within the long-lived positive ΔV_{oc} signal.

In a control experiment, designed to aid in the interpretation of the complex TPV data, we coated FTO electrodes with 3-SeP, without first depositing any $CuAlO_2$. Photovoltage transients for 3-SeP-functionalized FTO electrodes consisted of a negative ΔV_{oc} signal that decayed directly to baseline (Figure 3, inset B). The decay of the ΔV_{oc} was well-modeled by triexponential kinetics, with an amplitude-weighted average lifetime of 8.77×10^{-2} s (Appendix S1). A fit is superimposed on the measured photovoltage transient in Figure 3. We attribute the negative measured ΔV_{oc} signal to a negative shift of E_F of FTO arising from the injection of photoexcited electrons from 3-SeP to FTO. We have previously reported on the *n*-type sensitization of TiO_2-on-FTO electrodes by 3-SeP,[17,18] which necessarily implies that electron injection from 3-SeP to FTO is thermodynamically favorable.

https://doi.org/10.1021/acsaenm.4c00368
ACS Appl. Eng. Mater. 2024, 2, 2190−2200

Given the results of this control experiment, we likewise assign the initial short-lived negative ΔV_{oc} signal in photovoltage transients for 3-SeP/$CuAlO_2$-on-FTO electrodes (Figure 3, main graph) to electron injection from 3-SeP to FTO. In contrast, we attribute the subsequent and longer-lived positive ΔV_{oc} signal (0.1−0.9 s in Figure 3) to hole transfer from photoexcited 3-SeP to $CuAlO_2$, as depicted in Scheme 1. The injection of holes into $CuAlO_2$ should cause E_F of FTO to shift positively, as indeed measured in the TPV data. Notably, the absence of any positive signal for 3-SeP/FTO electrodes supports this assignment. Our TPV data thus provide compelling evidence in support of the excited-state hole-transfer mechanism that we targeted in developing 3-SeP-funcctionalized $CuAlO_2$ as a DSP.

Photoelectrochemical Characterization of 3-SeP-Functionalized $CuAlO_2$ Thin Films

To begin to evaluate whether excited-state hole transfer could be exploited in redox photocatalysis, we characterized 3-SeP/$CuAlO_2$-on-FTO electrodes using LSV. Prior to these measurements, we acquired cyclic voltammograms of bare FTO and $CuAlO_2$-on-FTO electrodes, with an electrolyte solution of $TBAPF_6$ (0.10 M) in CH_3CN, in the absence of illumination. At applied potentials from +0.50 to −0.30 V vs SCE, both FTO and $CuAlO_2$-on-FTO electrodes exhibited capacitive currents but negligible Faradaic currents (Figure S3 in Supporting Information), establishing this 800 mV range as an appropriate potential window for LSV measurements to evaluate photocurrent response.

We next acquired linear sweep voltammograms of FTO electrodes coated with either bare $CuAlO_2$ films or 3-SeP/$CuAlO_2$ films under chopped white-light (400−720 nm) illumination. These WEs were housed within sealed 3-compartment, 3-electrode cells with Pt mesh CE and SCE reference electrode (RE). The electrolyte was a CH_3CN solution of $TBAPF_6$ (0.10 M) and lactic acid (0.08 M), which served as a proton source and sacrificial electron donor. Unfunctionalized $CuAlO_2$-on-FTO WEs exhibited reductive photocurrents, as evidenced by the instantaneous increase of reductive current upon exposure of the WE to white light and the corresponding instantaneous decrease of reductive current when the light was blocked (Figure 4a). The magnitude of photocurrent density increased from approximately 0.3 μA cm^{-2} at an applied potential of +0.3 V vs SCE, to approximately 1.5 μA cm^{-2} at an applied potential of −0.25 V vs SCE. In contrast, 3-SeP/$CuAlO_2$-on-FTO WEs exhibited substantially greater reductive photocurrent densities, ranging from 1 to 18 μA cm^{-2} and increasing as the potential was swept negatively (Figure 4a). The inset to Figure 4a depicts average net photocurrent densities, calculated as the difference between the measured current density immediately after and before exposing WEs to white light, as a function of applied potential. At potentials from +0.2 to −0.3 V vs SCE, reductive photocurrents for 3-SeP/$CuAlO_2$-on-FTO WEs were 7-to-8-fold greater than those for $CuAlO_2$-on-FTO WEs. Notably, for both $CuAlO_2$-on-FTO and 3-SeP/$CuAlO_2$-on-FTO WEs, the onset of reductive photocurrent occurred at potentials several hundred millivolts more positive than the onset of dark reductive current, consistent with the reduction of photogenerated holes rather than ground-state holes. Thus, the energy of light was used to increase the reducing potential of the WE.

We performed two experiments to gain insight into the mechanism that produced reductive photocurrents. First, to evaluate the role of 3-SeP in light-harvesting, we acquired linear sweep voltammograms under illumination wherein the white light source was output through a notch filter that absorbed from 500 to 700 nm, the wavelength region in which 3-SeP absorbs most strongly (Figure 2), and we compared these data to linear sweep voltammograms acquired under full white-light (400−720 nm) illumination. (An absorptance spectrum of the notch filter is presented in Figure S4 in Supporting Information.) The goal of this experiment was to determine whether the mechanism giving rise to reductive photocurrent was initiated by excitation of 3-SeP, or, instead, whether photocurrent could be initiated by direct excitation of $CuAlO_2$. The LSV data are plotted in Figure 4b. Linear sweep voltammograms acquired under steady-state or chopped white-light illumination exhibited reductive photocurrents that increased with increasingly negative applied potentials, as outlined above. In contrast, linear sweep voltammograms acquired under steady-state, filtered illumination (i.e., from 400 to 500 nm and 700−720 nm) were essentially superimposable with LSV data acquired in the absence of any illumination. This result establishes that reductive photocurrents were initiated by photoexcitation of 3-SeP.

Second, we acquired chronocoulometry data for 3-SeP/$CuAlO_2$-on-FTO WEs, intermittently in the dark and under white-light (400−720 nm) illumination, within single-compartment cells with Pt CE and SCE RE. The charge passed between WE and CE was measured as a function of time at constant applied potential of −0.10 V vs SCE, a potential at which significant reductive photocurrents were measured in LSV experiments (Figure 4a,b). We acquired chronocoulometry data using four different electrolyte solutions, all of which contained $TBAPF_6$ (0.1 M) as supporting electrolyte: (1) Ar-purged electrolyte (to minimize the concentration of dissolved O_2) with dry CH_3CN as solvent (to minimize the concentration of H_2O), (2) air-equilibrated electrolyte (containing dissolved O_2) with dry CH_3CN as solvent, (3) Ar-purged electrolyte with 90:10 (v:v) CH_3CN/H_2O mixed solvent, and (4) air-equilibrated electrolyte with 90:10 (v:v) CH_3CN/H_2O mixed solvent. The goal of these experiments was to evaluate the importance of various possible reduction half-reactions at the 3-SeP/$CuAlO_2$ WE and oxidation half-reactions at the Pt CE, by measuring the charge passed in the presence and absence of potential electron- and hole-accepting solutes. During the acquisition of chhronocoulometry data, the WE was held in the dark for 5 min, then illuminated for 10 min, and this cycle was repeated for a total of 60 min. Chronocoulometry data are summarized in Figure 4c. For photoelectrochemical cells with electrolyte #1 (Ar-purged, dry CH_3CN), reductive charge (0.5−0.8 mC) was passed during the 10 min illumination periods, and oxidative charge (0.2−0.3 mC) was passed during the 5 min dark periods; this electrolyte was the only one for which any oxidation occurred at the WE. When O_2 was introduced into the electrolyte solution (electrolyte #2, air-equilibrated with dry CH_3CN), additional reductive charge (2−4 mC) was passed during the 10 min illumination periods, and essentially no charge was passed during the dark periods. The magnitude of reductive charge decreased with time across successive illumination periods. For electrolyte #3 (Ar-purged, 90:10 $CH_3CN:H_2O$), the reductive charge passed under illumination increased further (to 5−8 mC per 10 min illumination period) and was essentially

https://doi.org/10.1021/acsaenm.4c00368
ACS Appl. Eng. Mater. 2024, 2, 2190−2200

invariant over time; no charge was passed during the dark periods. Finally, for photoelectrochemical cells with electrolyte #4 (air-equilibrated, 90:10 CH_3CN:H_2O), the reductive charge passed during illumination was greatest (20−30 mC per 10 min illumination period), whereas much less reductive charge (2−3 mC) was passed in the dark. The reductive photocurrent decreased initially within the first illumination period but was invariant during subsequent illumination periods.

The results of these chronocoulometry experiments provide insight into the range of active reduction and oxidation half-reactions in these photoelectrochemical cells. In the absence of O_2 or H_2O (electrolyte #1), the minimal amount of reductive charge passed probably arose from reduction of 3-SeP and/or solvated H^+ from residual H_2O. The 4-to-10-fold increase of photoreductive charge passed with the addition of either O_2 (electrolyte #2) or H_2O (electrolyte #3), and the approximately 40-fold increase with the addition of both O_2 and H_2O (electrolyte #4), provide evidence that both O_2 and H^+ can be reduced by photoexcited 3-SeP. (We assume that H_2O was oxidized at the Pt CE.) Thus, taken together, the results of LSV and chronocoulometry measurements reveal (a) that photoinduced reduction reactions at 3-SeP/$CuAlO_2$-on-FTO WEs are initiated by excitation of the 3-SeP dye and (b) that photoexcited 3-SeP can reduce solvated species in the electrolyte, giving rise to sustainable reductive photocurrents when coupled with dark oxidation at the Pt CE.

Photoelectrochemical Hydrogen Evolution at 3-SeP/$CuAlO_2$ Photocathodes

Given that 3-SeP/$CuAlO_2$ can function as DSPs, we next sought to optimize their reactivity in the photocatalytic reduction of H^+ to H_2. To promote HER via the mechanism outlined in Scheme 1, we added Co-cat (Chart 1), as proton-reduction cocatalyst, and TEOA, as sacrificial electron donor, to the electrolyte.[21] In an initial experiment to assess whether TEOA was an effective electron donor to couple with reductive HER at the WE, we acquired chronocoulometry data for 3-SeP/$CuAlO_2$-on-FTO WEs, under white-light illumination, within 3-compartment electrochemical cells. The electrolyte solution in all three compartments contained Co-cat (1.0 mM) and KCl (0.10 M) in a 90:10 (v:v) CH_3CN/H_2O mixed solvent at pH 7.0. Chronocoulometry data were acquired when TEOA (0.38 M) was added to the electrolyte only in the WE compartment or only in the CE compartment, and also when TEOA was absent from both compartments. Photoelectrochemical cells with all three electrolyte compositions produced photocathodic currents and passed reductive charge during prolonged steady-state white-light illumination at an applied potential of −0.2 V vs SCE, revealing that the 3-SeP/$CuAlO_2$-on-FTO WEs functioned as DSPs under these conditions (Figure S4 in Supporting Information). When TEOA was present in the CE compartment, the total reductive charge passed after 1 h of illumination was 1.9-fold greater than when TEOA was present in the WE compartment and 1.7-fold greater than when it was altogether absent. The enhancement of reductive photocurrent when TEOA was present in the CE compartment, and the lack of an effect when TEOA was present in the WE compartment, provides evidence that TEOA was oxidized at the Pt CE, as outlined in Scheme 1, and thus that TEOA was indeed an effective sacrificial donor to promote photocathodic processes initiated by illumination of 3-SeP/$CuAlO_2$-on-FTO WEs.

Finally, we performed chronocoulometry experiments to evaluate HER at 3-SeP/$CuAlO_2$ DSPs, within 3-compartment cells with a Pt CE and SCE RE. The electrolyte consisted of Co-cat (1.0 mM), TEOA (0.38 M), and KCl (0.10 M) in a 90:10 (v:v) CH_3CN/H_2O mixed solvent. To promote HER, the electrolyte was acidified to pH 4 using HCl and was deaerated by purging with Ar for 30 min. Chronocoulometry data were acquired for 2−3 h under white-light illumination (with periodic dark periods to differentiate between light-initiated and dark electrochemical processes) at an applied potential ranging from −0.04 to −0.06 V vs SCE, at which reductive photocurrent was significant and dark current was negligible. After prolonged-illumination chronocoulometry measurements, the headspace above the electrolyte solution was characterized by gas chromatography (GC). Representative chronocoulometry data and gas chromatographs are shown in Figure 5. Under these conditions, the 3-SeP/

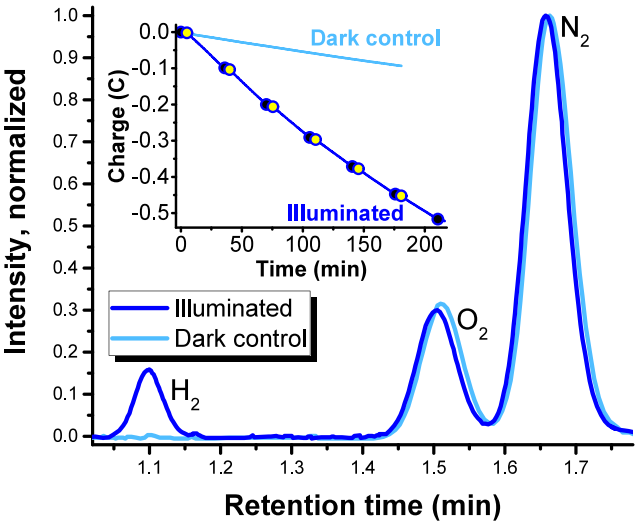

Figure 5. Gas chromatograph (royal blue trace) of the headspace above the electrolyte solution following 3-h white-light illumination of 3-SeP/$CuAlO_2$-on-FTO WEs at an applied potential of −0.04 V vs SCE, within a single-compartment cell with Pt CE; the electrolyte contained TEOA (0.38 M), KCl (0.10 M), and Co-cat (1.0 mM) in 90:10 (v:v) CH_3CN/H_2O. The light blue GC trace is from the headspace above the electrolyte from an unilluminated control sample. *Inset:* Corresponding chronocoulometry data for the illuminated and unilluminated samples. Every 30 min during the prolonged illumination, the light was blocked for 5 min, giving rise to plateaus in the data; black data points represent the start of dark periods, and yellow data points represent the start of illumination periods.

$CuAlO_2$ DSPs reproducibly passed reductive charge under illumination and produced gaseous H_2, as evidenced by the well-resolved peak at 1.1 min in the gas chromatograph. The average Faradaic efficiency for the reduction of H^+ to H_2 (eq S3 in Supporting Information), calculated from measurements on four different 3-SeP/$CuAlO_2$-on-FTO WEs, was (43 ± 27)%. In dark control experiments, the reductive charge passed was negligible (<1 mC), and H_2 was not detectable in the headspace by gas chromatography (Figure 5). The chronocoulometry data are thus consistent with the *p*-type sensitization mechanism in Scheme 1, in which HER is initiated by the transfer of holes from photoexcited 3-SeP to $CuAlO_2$. Photocatalytic HER over unfunctionalized $CuAlO_2$

https://doi.org/10.1021/acsaenm.4c00368
ACS Appl. Eng. Mater. 2024, 2, 2190−2200

has been reported,[54] and thus, in our measurements, some H_2 may have been produced following the direct excitation of $CuAlO_2$. However, given that our unfunctionalized $CuAlO_2$-on-FTO electrodes produced 7-to-8-fold lower photocurrents than 3-SeP/$CuAlO_2$-on-FTO electrodes (Figure 4a), we conclude that the significant majority of HER was initiated by excitation of 3-SeP. We tentatively attribute the sub-100% Faradaic efficiency for HER to the reduction of 3-SeP and/or Co-cat. Our measured Faradaic efficiencies for photocatalytic HER are similar to those recently reported by Reisner and co-workers for $CuCrO_2$-derived DSPs with organic dyes and a Ni(II) cocatalyst[13,14] but lower than the Faradaic efficiency reported by Windle et al. for a Z-scheme photoelectrochemical cell incorporating a $CuGaO_2$-derived DSP with an organic dye and a Co(III) cocatalyst.[12]

CONCLUSIONS

We have reported on the attachment of 3-SeP to $CuAlO_2$ thin films and the characterization of light-initiated charge transfer and redox chemistry including HER via the reduction of H^+ to H_2. Several factors render 3-SeP-functionalized $CuAlO_2$ as a promising DSP architecture. First, 3-SeP absorbs light at lower energies than analogous O-containing rhodamines and undergoes efficient intersystem crossing to yield a long-lived excited-state that enables interfacial hole transfer to compete more efficiently with electron−hole recombination. Second, $CuAlO_2$, like other Cu(I) delafossites, has an unusually high-energy valence band edge and high hole mobility. Third, the phosphonate linkage between 3-SeP and $CuAlO_2$ is particularly inert, and 3-SeP adsorbs to $CuAlO_2$ as a mixture of monomeric and H-aggregated dyes, which broadens the dye's absorption bands and increases visible light harvesting. Our TPV, LSV, and chronocoulometry data reveal that photoexcited 3-SeP transfers holes to $CuAlO_2$, which separates holes from electrons and enables subsequent oxidation and reduction half reactions. The TPV data, in particular, provide compelling evidence that photoexcited 3-SeP dyes transfer holes to $CuAlO_2$. Our results thus reveal that selenorhodamine dyes can function as *p*-type sensitizers. Notably, 3-SeP/$CuAlO_2$ DSPs significantly outperformed unfunctionalized $CuAlO_2$ photocathodes, highlighting the importance of the hole-transfer mechanism in redox photocatalysis. In conjunction with a Co(III) cocatalyst and a sacrificial donor, 3-SeP/$CuAlO_2$ DSPs reduced H^+ to H_2 with Faradaic efficiency of approximately 40%. Our results highlight the potential of selenorhodamine-sensitized $CuAlO_2$ as a DSP architecture for solar photocatalysis. Ongoing challenges and opportunities include improving the efficiency of HER, evaluating and maximizing the longevity of photocatalytic performance, coupling the reduction of H^+ with the oxidation of H_2O or other nonsacrificial donors, and exploring alternative redox photocatalytic mechanisms. Finally, dissolution of the cobaloxime reduction cocatalyst in the electrolyte solution is not practical and probably limits photocatalytic performance. Co-immobilization of dyes and cocatalysts on $CuAlO_2$ may render this class of DSPs more suitable for real-world applications, and we are exploring this possibility.

ASSOCIATED CONTENT

Supporting Information

The Supporting Information is available free of charge at https://pubs.acs.org/doi/10.1021/acsaenm.4c00368.

EDS spectra, SEM images, and cyclic voltammetry data for $CuAlO_2$, chronocoulometry data for 3-SeP-functionalized $CuAlO_2$, and descriptions of the estimation of surface coverages of dyes on $CuAlO_2$, multiexponential fitting of photovoltage transients and the calculation of Faradaic efficiencies of hydrogen evolution (PDF)

AUTHOR INFORMATION

Corresponding Authors

Kacie Liwosz − *Department of Natural Science and Mathematics, D'Youville University, Buffalo, New York 14201, United States;* orcid.org/0000-0001-6582-8317; Email: liwoszk@dyc.edu

David F. Watson − *Department of Chemistry, University at Buffalo, The State University of New York, Buffalo, New York 14260-3000, United States;* orcid.org/0000-0003-1203-2811; Phone: 716-645-4189; Email: dwatson3@buffalo.edu

Authors

Michael D. Clark − *Department of Chemistry, University at Buffalo, The State University of New York, Buffalo, New York 14260-3000, United States;* orcid.org/0000-0002-5232-546X

Zachery A. Schmidt − *Department of Chemistry, University at Buffalo, The State University of New York, Buffalo, New York 14260-3000, United States*

Gregory J. Lapp − *Department of Natural Science and Mathematics, D'Youville University, Buffalo, New York 14201, United States*

Hannah R. Dierolf − *Department of Natural Science and Mathematics, D'Youville University, Buffalo, New York 14201, United States*

Complete contact information is available at: https://pubs.acs.org/10.1021/acsaenm.4c00368

Funding

National Science Foundation Grant CHE-1900272.

Notes

The authors declare no competing financial interest.

ACKNOWLEDGMENTS

This material is based upon work supported by the National Science Foundation under Grant no. CHE-1900272. Additional support was provided by the University at Buffalo. SEM, EDS, and XRD data were acquired using resources of the South Campus Instrument Center of the University at Buffalo. We thank our colleague and mentor, the late Prof. Michael Detty, for his guidance on the synthesis and photophysical properties of selenorhodamine dyes. We thank Isabelle Prentice and Jenna Davies for assistance in performing dye-desorption experiments.

REFERENCES

(1) Yu, M.; Draskovic, T. I.; Wu, Y. Cu(I)-Based Delafossite Compounds as Photocathodes in P-Type Dye-Sensitized Solar Cells. *Phys. Chem. Chem. Phys.* **2014**, *16*, 5026−5033.

(2) Nikolaou, V.; Charisiadis, A.; Charalambidis, G.; Coutsolelos, A. G.; Odobel, F. Recent Advances and Insights in Dye-Sensitized NiO Photocathodes for Photovoltaic Devices. *J. Mater. Chem. A* **2017**, *5*, 21077−21113.

(3) Odobel, F.; Pellegrin, Y. Recent Advances in the Sensitization of Wide-Band-Gap Nanostructured P-Type Semiconductors. Photovoltaic and Photocatalytic Applications. *J. Phys. Chem. Lett.* **2013**, *4*, 2551−2564.
(4) Gibson, E. A. Dye-Sensitized Photocathodes for H_2 Evolution. *Chem. Soc. Rev.* **2017**, *46*, 6194−6209.
(5) Odobel, F.; Pellegrin, Y.; Gibson, E. A.; Hagfeldt, A.; Smeigh, A. L.; Hammarström, L. Recent Advances and Future Directions to Optimize the Performances of P-Type Dye-Sensitized Solar Cells. *Coord. Chem. Rev.* **2012**, *256*, 2414−2423.
(6) Muñoz-García, A. B.; Benesperi, I.; Boschloo, G.; Concepcion, J. J.; Delcamp, J. H.; Gibson, E. A.; Meyer, G. J.; Pavone, M.; Pettersson, H.; Hagfeldt, A.; Freitag, M. Dye-Sensitized Solar Cells Strike Back. *Chem. Soc. Rev.* **2021**, *50*, 12450−12550.
(7) Benazzi, E.; Mallows, J.; Summers, G. H.; Black, F. A.; Gibson, E. A. Developing Photocathode Materials for P-Type Dye-Sensitized Solar Cells. *J. Mater. Chem. C* **2019**, *7*, 10409−10445.
(8) Dalle, K. E.; Warnan, J.; Leung, J. J.; Reuillard, B.; Karmel, I. S.; Reisner, E. Electro- and Solar-Driven Fuel Synthesis with First Row Transition Metal Complexes. *Chem. Rev.* **2019**, *119*, 2752−2875.
(9) Wrede, S.; Tian, H. Towards Sustainable and Efficient P-Type Metal Oxide Semiconductor Materials in Dye-Sensitised Photocathodes for Solar Energy Conversion. *Phys. Chem. Chem. Phys.* **2020**, *22*, 13850−13861.
(10) Sullivan, I.; Zoellner, B.; Maggard, P. A. Copper(I)-Based P-Type Oxides for Photoelectrochemical and Photovoltaic Solar Energy Conversion. *Chem. Mater.* **2016**, *28*, 5999−6016.
(11) Kumagai, H.; Sahara, G.; Maeda, K.; Higashi, M.; Abe, R.; Ishitani, O. Hybrid Photocathode Consisting of a $CuGaO_2$ P-Type Semiconductor and a Ru(II)−Re(I) Supramolecular Photocatalyst: Non-Biased Visible-Light-Driven CO_2 Reduction with Water Oxidation. *Chem. Sci.* **2017**, *8*, 4242−4249.
(12) Windle, C. D.; Kumagai, H.; Higashi, M.; Brisse, R.; Bold, S.; Jousselme, B.; Chavarot-Kerlidou, M.; Maeda, K.; Abe, R.; Ishitani, O.; Artero, V. Earth-Abundant Molecular Z-Scheme Photoelectrochemical Cell for Overall Water-Splitting. *J. Am. Chem. Soc.* **2019**, *141*, 9593−9602.
(13) Creissen, C. E.; Warnan, J.; Antón-García, D.; Farré, Y.; Odobel, F.; Reisner, E. Inverse Opal $CuCrO_2$ Photocathodes for H_2 Production Using Organic Dyes and a Molecular Ni Catalyst. *ACS Catal.* **2019**, *9*, 9530−9538.
(14) Creissen, C. E.; Warnan, J.; Reisner, E. Solar H_2 Generation in Water with a $CuCrO_2$ Photocathode Modified with an Organic Dye and Molecular Ni Catalyst. *Chem. Sci.* **2018**, *9*, 1439−1447.
(15) Mann, J. R.; Gannon, M. K.; Fitzgibbons, T. C.; Detty, M. R.; Watson, D. F. Optimizing the Photocurrent Efficiency of Dye-Sensitized Solar Cells through the Controlled Aggregation of Chalcogenoxanthylium Dyes on Nanocrystalline Titania Films. *J. Phys. Chem. C* **2008**, *112*, 13057−13061.
(16) Mulhern, K. R.; Detty, M. R.; Watson, D. F. Aggregation-Induced Increase of the Quantum Yield of Electron Injection from Chalcogenorhodamine Dyes to TiO_2. *J. Phys. Chem. C* **2011**, *115*, 6010−6018.
(17) Mulhern, K. R.; Orchard, A.; Watson, D. F.; Detty, M. R. Influence of Surface-Attachment Functionality on the Aggregation, Persistence, and Electron-Transfer Reactivity of Chalcogenorhodamine Dyes on TiO_2. *Langmuir* **2012**, *28*, 7071−7082.
(18) Mulhern, K. R.; Detty, M. R.; Watson, D. F. Effects of Surface-Anchoring Mode and Aggregation State on Electron Injection from Chalcogenorhodamine Dyes to Titanium Dioxide. *J. Photochem. Photobiol., A* **2013**, *264*, 18−25.
(19) Sabatini, R. P.; Eckenhoff, W. T.; Orchard, A.; Liwosz, K. R.; Detty, M. R.; Watson, D. F.; McCamant, D. W.; Eisenberg, R. From Seconds to Femtoseconds: Solar Hydrogen Production and Transient Absorption of Chalcogenorhodamine Dyes. *J. Am. Chem. Soc.* **2014**, *136*, 7740−7750.
(20) Kryman, M. W.; Nasca, J. N.; Watson, D. F.; Detty, M. R. Selenorhodamine Dye-Sensitized Solar Cells: Influence of Structure and Surface-Anchoring Mode on Aggregation, Persistence, and Photoelectrochemical Performance. *Langmuir* **2016**, *32*, 1521−1532.
(21) McCormick, T. M.; Calitree, B. D.; Orchard, A.; Kraut, N. D.; Bright, F. V.; Detty, M. R.; Eisenberg, R. Reductive Side of Water Splitting in Artificial Photosynthesis: New Homogeneous Photosystems of Great Activity and Mechanistic Insight. *J. Am. Chem. Soc.* **2010**, *132*, 15480−15483.
(22) Ohulchanskyy, T. Y.; Donnelly, D. J.; Detty, M. R.; Prasad, P. N. Heteratom Substitution Induced Changes in Excited-State Photophysics and Singlet Oxygen Generation in Chalcogenoxanthylium Dyes: Effect of Sulfur and Selenium Substitutions. *J. Phys. Chem. B* **2004**, *108*, 8668−8672.
(23) Rajeshwar, K.; Hossain, M. K.; Macaluso, R. T.; Janáky, C.; Varga, A.; Kulesza, P. J. Review—Copper Oxide-Based Ternary and Quaternary Oxides: Where Solid-State Chemistry Meets Photoelectrochemistry. *J. Electrochem. Soc.* **2018**, *165*, H3192.
(24) Schiavo, E.; Latouche, C.; Barone, V.; Crescenzi, O.; Muñoz-García, A. B.; Pavone, M. An Ab Initio Study of Cu-Based Delafossites as an Alternative to Nickel Oxide in Photocathodes: Effects of Mg-Doping and Surface Electronic Features. *Phys. Chem. Chem. Phys.* **2018**, *20*, 14082−14089.
(25) Kawazoe, H.; Yasukawa, M.; Hyodo, H.; Kurita, M.; Yanagi, H.; Hosono, H. P-Type Electrical Conduction in Transparent Thin Films of $CuAlO_2$. *Nature* **1997**, *389*, 939−942.
(26) Das, B.; Renaud, A.; Volosin, A. M.; Yu, L.; Newman, N.; Seo, D.-K. Nanoporous Delafossite $CuAlO_2$ from Inorganic/Polymer Double Gels: A Desirable High-Surface-Area P-Type Transparent Electrode Material. *Inorg. Chem.* **2015**, *54*, 1100−1108.
(27) Jarman, R. H.; Bafia, J.; Gebreslasse, T.; Ingram, B. J.; Carter, J. D. Synthesis of the P-Type Semiconducting Ternary Oxide $CuAlO_2$ Using the Pechini Method. *Mater. Res. Bull.* **2013**, *48*, 3916−3918.
(28) Nattestad, A.; Zhang, X.; Bach, U.; Cheng, Y.-B. Dye-Sensitized $CuAlO_2$ Photocathodes for Tandem Solar Cell Applications. *J. Photonics Energy* **2011**, *1*, No. 011103.
(29) Deng, Z.; Zhu, X.; Tao, R.; Dong, W.; Fang, X. Synthesis of $CuAlO_2$ Ceramics Using Sol-Gel. *Mater. Lett.* **2007**, *61*, 686−689.
(30) Ahmed, J.; Blakely, C. K.; Prakash, J.; Bruno, S. R.; Yu, M.; Wu, Y.; Poltavets, V. V. Scalable Synthesis of Delafossite $CuAlO_2$ Nanoparticles for P-Type Dye-Sensitized Solar Cells Applications. *J. Alloys Compd.* **2014**, *591*, 275−279.
(31) Bandara, J.; Yasomanee, J. P. P-Type Oxide Semiconductors as Hole Collectors in Dye-Sensitized Solid-State Solar Cells. *Semicond. Sci. Technol.* **2007**, *22*, 20−24.
(32) Del Valle, D. J.; Donnelly, D. J.; Holt, J. J.; Detty, M. R. 2,7-Bis-N,N-Dimethylaminochalcogenoxanthen-9-Ones Via Electrophilic Cyclization with Phosphorus Oxychloride. *Organometallics* **2005**, *24*, 3807−3810.
(33) Gannon, M. K. I.; Detty, M. R. Generation of 3- and 5-Lithiothiophene-2-Carboxylates Via Metal-Halogen Exchange and Their Addition Reactions to Chalcogenoxanthones. *J. Org. Chem.* **2007**, *72*, 2647−2650.
(34) Watson, D. F.; Meyer, G. J. Electron Injection at Dye-Sensitized Semiconductor Electrodes. *Annu. Rev. Phys. Chem.* **2005**, *56*, 119−156.
(35) Gerischer, H. Semiconductor Electrochemistry. In *Physical Chemistry: An Advanced Treatise*, Eyring, H., Henderson, D., Jost, W., Eds.; Vol. *9A*; Academic Press, 1970; pp 463−542.
(36) Benko, F. A.; Koffyberg, F. P. Opto-Electronic Properties of $CuAlO_2$. *J. Phys. Chem. Solids* **1984**, *45*, 57−59.
(37) Williamson, B. A. D.; Buckeridge, J.; Chadwick, N. P.; Sathasivam, S.; Carmalt, C. J.; Parkin, I. P.; Scanlon, D. O. Dispelling the Myth of Passivated Codoping in TiO_2. *Chem. Mater.* **2019**, *31*, 2577−2589.
(38) Sabatini, R. P.; Mark, M. F.; Mark, D. J.; Kryman, M. W.; Hill, J. E.; Brennessel, W. W.; Detty, M. R.; Eisenberg, R.; McCamant, D. W. A Comparative Study of the Photophysics of Phenyl, Thienyl, and Chalcogen Substituted Rhodamine Dyes. *Photochem. Photobiol. Sci.* **2016**, *15*, 1417−1432.

https://doi.org/10.1021/acsaenm.4c00368
ACS Appl. Eng. Mater. 2024, 2, 2190−2200

(39) Clark, W. D. K.; Sutin, N. Spectral Sensitization of N-Type TiO_2 Electrodes by Polypyridineruthenium(II) Complexes. *J. Am. Chem. Soc.* **1977**, *99*, 4676−4682.
(40) Bangle, R. E.; Schneider, J.; Piechota, E. J.; Troian-Gautier, L.; Meyer, G. J. Electron Transfer Reorganization Energies in the Electrode−Electrolyte Double Layer. *J. Am. Chem. Soc.* **2020**, *142*, 674−679.
(41) Pechini, M. P. Method of Preparing Lead and Alkaline Earth Titanates and Niobates and Coating Method Using the Same to Form a Capacitor. US33306971967
(42) Segal, D. Chemical Synthesis of Ceramic Materials. *J. Mater. Chem.* **1997**, *7*, 1297−1305.
(43) Kakihana, M.; Yoshimura, M. Synthesis and Characteristics of Complex Multicomponent Oxides Prepared by Polymer Complex Method. *Bull. Chem. Soc. Jpn.* **1999**, *72*, 1427−1443.
(44) Ishiguro, T.; Kitazawa, A.; Mizutani, N.; Kato, M. Single-Crystal Growth and Crystal Structure Refinement of Cualo2. *J. Solid State Chem.* **1981**, *40*, 170−174.
(45) Kasha, M.; Rawls, H. R.; Ashraf El-Bayoumi, M. The Exciton Model in Molecular Spectroscopy. *Pure Appl. Chem.* **1965**, *11*, 371−392.
(46) López Arbeloa, F.; Martínez Martínez, V.; Arbeloa, T.; López Arbeloa, I. Photoresponse and Anisotropy of Rhodamine Dye Intercalated in Ordered Clay Layered Films. *J. Photochem. Photobiol. C* **2007**, *8*, 85−108.
(47) Fatihi, M. Y.; Gueddida, S.; Hasnaoui, A.; Lebègue, S.; Pastore, M. First-Principles Modeling of the Adsorption Mechanism of Carboxylic and Phosphonic Acids onto Pristine and Defective Delafossite $CuAlO_2$ Surfaces. *Phys. Stat. Solidi (B)* **2023**, *260*, 2200611.
(48) Trammell, S. A.; Moss, J. A.; Yang, J. C.; Nakhle, B. M.; Slate, C. A.; Odobel, F.; Sykora, M.; Erickson, B. W.; Meyer, T. J. Sensitization of Tio_2 by Phosphonate-Derivatized Proline Assemblies. *Inorg. Chem.* **1999**, *38*, 3665−3669.
(49) Gao, W.; Dickinson, L.; Grozinger, C.; Morin, F. G.; Reven, L. Self-Assembled Monolayers of Alkylphosphonic Acids on Metal Oxides. *Langmuir* **1996**, *12*, 6429−6435.
(50) Shuttle, C. G.; O'Regan, B.; Ballantyne, A. M.; Nelson, J.; Bradley, D. D. C.; de Mello, J.; Durrant, J. R. Experimental Determination of the Rate Law for Charge Carrier Decay in a Polythiophene: Fullerene Solar Cell. *Appl. Phys. Lett.* **2008**, *92*, No. 093311.
(51) Barnes, P. R. F.; Miettunen, K.; Li, X.; Anderson, A. Y.; Bessho, T.; Gratzel, M.; O'Regan, B. C. Interpretation of Optoelectronic Transient and Charge Extraction Measurements in Dye-Sensitized Solar Cells. *Adv. Mater.* **2013**, *25*, 1881−1922.
(52) Bisquert, J.; Fabregat-Santiago, F.; Mora-Seró, I.; Garcia-Belmonte, G.; Giménez, S. Electron Lifetime in Dye-Sensitized Solar Cells: Theory and Interpretation of Measurements. *J. Phys. Chem. C* **2009**, *113*, 17278−17290.
(53) Sandberg, O. J.; Tvingstedt, K.; Meredith, P.; Armin, A. Theoretical Perspective on Transient Photovoltage and Charge Extraction Techniques. *J. Phys. Chem. C* **2019**, *123*, 14261−14271.
(54) Koriche, N.; Bouguelia, A.; Aider, A.; Trari, M. Photocatalytic Hydrogen Evolution over Delafossite $CuAlO_2$. *Int. J. Hydrogen Energy* **2005**, *30*, 693−699.

https://doi.org/10.1021/acsaenm.4c00368
ACS Appl. Eng. Mater. 2024, 2, 2190−2200